Morphology dependent adsorption of methylene blue on trititanate nanoplates and nanotubes prepared by the hydrothermal treatment of TiO_2

Graham Dawson, Wei Chen, Luhua Lu and Kai Dai

ABSTRACT

The adsorption properties of two nanomorphologies of trititanate, nanotubes (TiNT) and plates (TiNP), prepared by the hydrothermal reaction of concentrated NaOH with different phases of TiO_2, were examined. It was found that the capacity for both morphologies towards methylene blue (MB), an ideal pollutant, was extremely high, with the TiNP having a capacity of 130 mg/g, higher than the TiNT, whose capacity was 120 mg/g at 10 mg/L MB concentration. At capacity, the well-dispersed powders deposit on the floor of the reaction vessel. The two morphologies had very different structural and adsorption properties. TiNT with high surface area and pore volume exhibited exothermic monolayer adsorption of MB. TiNP with low surface area and pore volume yielded a higher adsorption capacity through endothermic multilayer adsorption governed by pore diffusion. TiNP exhibited a higher negative surface charge of −23 mV, compared to −12 mV for TiNT. The adsorption process appears to be an electrostatic interaction, with the cationic dye attracted more strongly to the nanoplates, resulting in a higher adsorption capacity and different adsorption modes. We believe this simple, low cost production of high capacity nanostructured adsorbent material has potential uses in wastewater treatment.

Key words | adsorption, methylene blue, trititanate nanotubes

Graham Dawson (corresponding author)
Department of Chemistry,
Xi'an Jiaotong Liverpool University,
111 Renai Road, Dushu Lake Higher Education Town, Suzhou Industrial Park,
Suzhou,
Jiangsu 215123,
China
E-mail: *graham.dawson@xjtlu.edu.cn*

Wei Chen
i-lab, Suzhou Institute of Nanotechnology and Nanobionics, Chinese Academy of Sciences,
Dushu Lake Higher Education Town, Suzhou Industrial Park,
Suzhou,
Jiangsu 215123,
China

Luhua Lu
China Faculty of Material Science and Chemical Engineering,
China University of Geosciences,
Wuhan 430074,
China

Kai Dai
College of Physics and Electronic Information, Huaibei Normal University,
Huaibei 235000,
China

INTRODUCTION

Dye compounds are common and difficult to remove pollutants from several industries, including textiles and printing. The removal of dye compounds from wastewater has therefore received considerable attention in recent years and requires environmentally friendly materials and potentially easy separation or regeneration techniques (Ramakrishna & Viraraghavan 1997; Crini 2006). Photocatalytic and biological degradations of the dyestuffs can result in the production of toxic products due to the complex nature of the aromatic dye molecules, therefore adsorption is a promising technique for the removal of dyes from water (Zhao & Liu 2008). A wide variety of adsorbents have been employed for several different applications, including activated carbon and mesoporous molecular sieves, however, the operating and regeneration costs are high, leading to a search for low cost, high capacity absorbents (Widjaja *et al.* 2004; Namane *et al.* 2005; Parida *et al.* 2006; Wang *et al.* 2006). Nanostructured materials are of great interest due to their exceptional electronic and mechanical properties, as well as exhibiting high surface areas: a useful property for adsorption. Research pertaining to inorganic nanotubes has been extensive (Tenne *et al.* 1992; Feldman *et al.* 1995; Nakamuara & Matsui 1995; Hoyer 1996; Pu *et al.* 2001; Goldberger *et al.* 20013), with TiO_2 receiving a great deal of attention.

Titania nanotubes were first prepared by the hydrothermal treatment of TiO_2 with 10 M NaOH (Kasuga *et al.* 1998). The nanotubular material was produced by treating crystalline TiO_2 with 10 molar NaOH. It was concluded that washing the alkali treated specimen with water followed by further reaction with HCl are vital steps in the formation of nanotubes (Kasuga *et al.* 1999). Work has later shown (Chen *et al.* 2002) that the nanotubes could be prepared

doi: 10.2166/wst.2016.519

via a single hydrothermal alkali treatment of crystalline TiO_2.

We have shown that the reaction temperature and phase composition of the starting material are important factors in determining the morphology of the product (Dawson *et al.* 2010). The anatase component of the starting material is easily converted to trititanate nanotubes at 140 °C, where, as the rutile, remains unreacted. After the temperature is increased to 170 °C, the morphology is exclusively trititanate nanoplates, with the tubular structure destroyed. The high adsorption capacity of trititanate nanotubes for basic dyes has been reported (Lee *et al.* 2007; Hsieh *et al.* 2008), with the dye is adsorbed on the nanotube via an ion exchange mechanism. Modification of the nanotube surface by dopamine imparts photocatalytic properties on the composite material (Dawson *et al.* 2012; Liu *et al.* 2016), however little is known about the adsorption process and interaction.

In this study, we have compared the adsorption properties of trititanate tubes and plates prepared by the hydrothermal treatment of different phase TiO_2. It was found that nanotubes with high surface area and pore volume exhibited exothermic monolayer adsorption of methylene blue (MB) governed by external mass transport. Nanoplates with low surface area and pore volume yielded a higher adsorption capacity through endothermic multilayer adsorption governed by pore diffusion. We believe these nanostructured materials have interesting potential applications in wastewater treatment and absorption.

EXPERIMENTAL

Preparation of nanostructures

The two different nanostructures were prepared following our previously reported method (Dawson *et al.* 2010) at 140 °C for 72 h for anatase (TiNT) and 170 °C for seven days for rutile (TiNP).

Characterisation

The products morphologies were investigated using field emission scanning electron microscopy (FESEM) (FEI Quanta 400 FEG) and transmission electron microscopy (TEM) (FEI Tecnai F20 operating at 200 kV). Powder X-ray diffraction (XRD) was performed with CuKα radiation on a X'Pert Pro MPD operation at 40 kV and 30 mA. Zeta potentials were measured using a Colloidal Dynamics Zeta Probe. Specific surface areas, pore size and pore volumes were determined by nitrogen adsorption at −196 °C on a Micromeritics ASAP 2020 apparatus. The surface area was determined by the Brunauer–Emmett–Teller (BET) method.

The adsorption capacity of the samples was investigated with MB dye solution. Sample powder (0.01 g) was suspended in 100 mL of MB solution of the desired concentration. The reaction mixture was placed in an incubator shaker equipped with a constant temperature controller at 100 rpm for 5 h. After the adsorption period, an amount of solution was centrifuged at 120,000 rpm for 20 min. The concentration of MB left in solution was determined using a UV spectrometer (Perkin Elmer Lambda 25) at 665 nm by comparing the absorbance against a standardised calibration curve. The amount of dye adsorbed on the sample was calculated from the concentration of dye left in the solution using Equation (1):

$$Q = \frac{V(C_i - C_e)}{M} \tag{1}$$

where Q is the adsorption capacity (mg/g), C_i is the initial concentration of methylene blue, C_e is the equilibrium concentration, V is the volume of solution and M is the mass of Ti sample in the reaction.

Adsorption isotherms

The equilibrium adsorption isotherms were analysed using the Langmuir and BET models.

The Langmuir model can be described by the following form:

$$Q_e = \frac{Q_m K_L C_e}{1 + K_L C_e} \tag{2}$$

where Q_e (mg/g) is the solid phase equilibrium concentration, Q_m (mg/g) is the maximum adsorption capacity, K_L (L/mg) is the Langmuir constant and C_e (mg/L) is the liquid phase equilibrium concentration.

The model assumes that adsorption occurs on a homogenous surface of identical sites that are equally available and energetically equivalent and each site carries equal numbers of molecules with no interaction between adsorbate molecules. The linear form of the Langmuir equation can be represented as follows:

$$\frac{C_e}{Q_e} = \frac{1}{Q_m K_L} + \frac{C_e}{Q_m} \tag{3}$$

Therefore, if the model is valid a linear plot of C_e/Q_e versus C_e will yield K_L and Q_m from the intercept and slope.

The BET isotherm is given below in the linear form:

$$\frac{M.C}{(C_s - C)x} = \frac{1}{AX_m} + \frac{(A-1)}{AX_m}\frac{C}{C_s} \quad (4)$$

where M is the mass of adsorber (mg), C_s is the saturation concentration, X_m is the BET monolayer capacity and A is a constant.

For adsorption from the liquid phase, the partial pressure term can be replaced by the saturation concentration (Parker 1995). In this study, we have used the initial concentration of MB, C_i, in accordance with (El-Halwany 2010). Thus, plotting $M.C/(C_s\text{-}C)x$ versus C/C_s will give rise to a straight line from whose slope and intercept the BET monolayer can be calculated. The value of the correlation coefficient, r^2, determines which model is the best fit for the data.

Thermodynamic parameters

The adsorption isotherms were measured at three temperatures, so the heat of adsorption can be calculated. The temperature dependency of the adsorption equilibrium constant K (Q_e/C_e) obeyed the van't Hoff equation:

$$\frac{d\ln K}{dT} = \frac{\Delta H}{RT^2} \quad (5)$$

which, when integrated, gives:

$$\ln K = \ln K_0 + (-\Delta H/RT) \quad (6)$$

The value of ΔH can be determined from the slope of the plot of lnK versus 1/T, which produces a straight line.

The Gibbs free energy, ΔG (J/mol), is an indication of the spontaneity of a chemical reaction. If the value of ΔG has a negative value the reaction will proceed spontaneously. For an adsorption reaction it is given by the following equation:

$$\Delta G = -RT\ln K \quad (7)$$

The entropy change can also then be calculated using the following equation:

$$\Delta G = \Delta H - T\Delta S \quad (8)$$

Kinetics

The kinetic data were analysed using the linear form of the pseudo-second-order kinetic model proposed by Ho, which has been extensively used to predict dye adsorption kinetics (Ho & McKay 1999):

$$\frac{t}{Q_t} = \frac{1}{k_{ps}Q_e^2} + \frac{t}{Q_e} \quad (9)$$

where k_{ps} (g/mg h) is the pseudo-second-order rate constant. A plot of t/Q_t versus time will yield a straight line if the pseudo-second-order model is valid, with the values of k_{ps} and Q_e calculated from the slope and intercept.

The adsorption was further investigated using the intraparticle diffusion model given below, which examines the steps involved during adsorption:

$$Q_t = k_d t^{1/2} \quad (10)$$

A two-phase plot would suggest that the adsorption proceeds by external mass transfer (boundary layer diffusion) described by the curved section of the plot, and intraparticle, or pore, diffusion described by the linear section.

RESULTS AND DISCUSSION

Structural properties of nanotubes and nanoplates

Two distinct morphologies of trititanate, nanotubes and nanoplates, were prepared from TiO_2 according to our previous report. The morphological and structural properties are summarised in Figure 1 and Table 1. A detailed study of the morphology and synthesis can be found in our previous report (Dawson *et al.* 2010).

The specific surface area and pore volumes of the two samples were measured using the BET and Barrett–Joyner–Halenda (BJH) methods, respectively. The surface area of TiNT was found to be 250 m^2/g. The TiNP sample exhibited a surface area of 40 m^2/g, much lower than the tube sample. In the TiNT sample, the pore size peak at 3.4 nm is attributed to the internal tube cavity, which is in agreement with the TEM observations (Figure 1). The pore distribution is wide, with the larger pores between 10 and 100 nm being attributed to voids formed between nanotube aggregates. The distribution for the TiNP sample is also large, with small pore peaks at 2.1 and 3.7 nm. From the TEM shown in Figure 1,

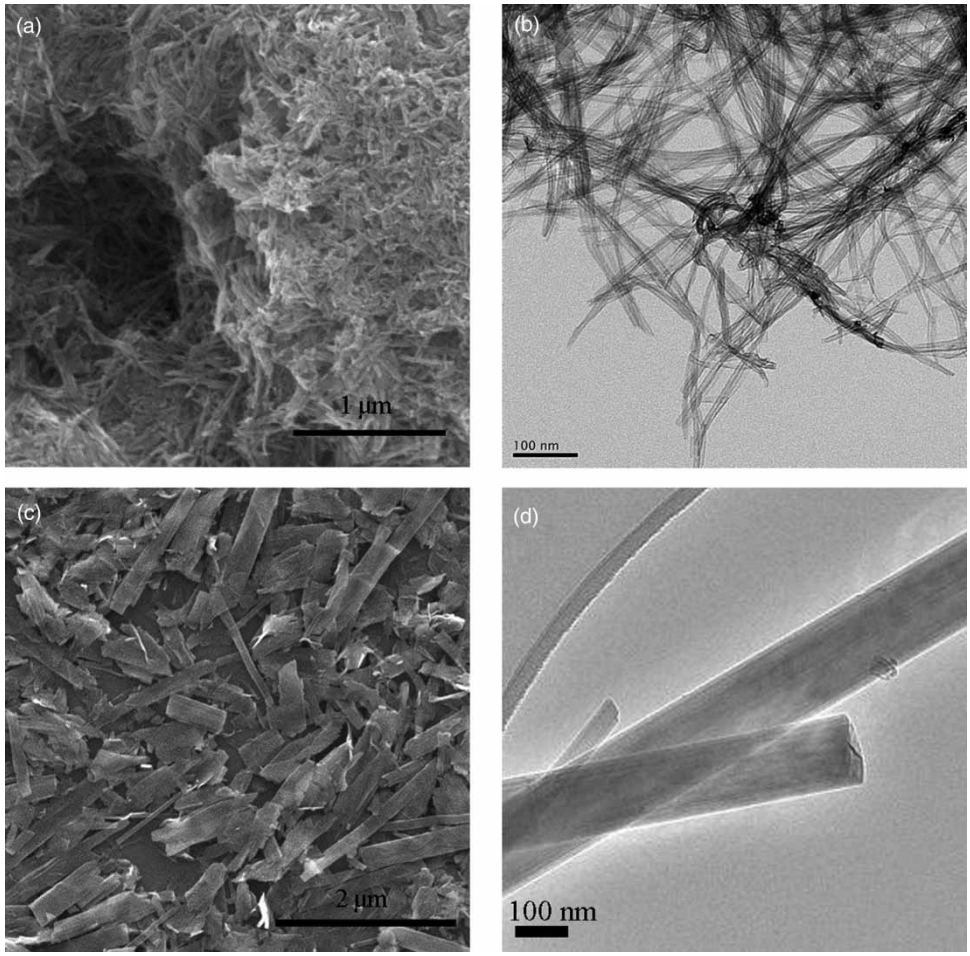

Figure 1 | Scanning electron microscopy (SEM) and transmission electron microscopy (TEM) images of TiNT (a) and (b) and TiNP (c) and (d).

Table 1 | Surface properties for TiNT and TiNP

Sample	BET surface area (m^2/g)	Pore volume (cm^3/g)	Average pore size (nm)	Zeta potential (mV)	Experimental adsorption capacity (mg/g)
TiNT	249.4	0.945	13.1	−12	120
TiNP	40.1[a]	0.19[a]	18.1[a]	−23	130

[a]From ref [17].

we can see that there are no pores visible in the plate structures themselves, so it can be concluded that the mesopores come from the aggregation and stacking of plates, with the larger pores created in the voids between the particles. The pore volume for TiNT was high, 0.9 cm^3/g, but TiNP had a low pore volume of 0.19 cm^3/g.

The stability of the samples in aqueous solution was measured by zeta potential, and are shown in Table 1. TiNT had a potential of −12 mV at a pH of 6.7, and TiNP exhibited a value of −23 mV at pH 6.0. TiNP exhibit a higher –ve zeta potential, and are therefore more stable in suspension.

The adsorption characteristics and kinetics of the two morphologies were compared and are detailed below.

Liquid phase adsorption of MB

The adsorption isotherms of TiNT and TiNP for MB uptake at different temperatures are shown in Figure 2. They were analysed according to the linear forms of the Langmuir and BET isotherms and the parameters k_L and Q_e from the Langmuir model and A and X_m from the BET model were calculated and listed in Table 2 along with the correlation coefficients, r^2.

As can be seen, the Langmuir model is a good fit for the TiNT data, with all r^2 values >0.99. While the Langmuir model reflects monolayer adsorption, a good fit to the BET

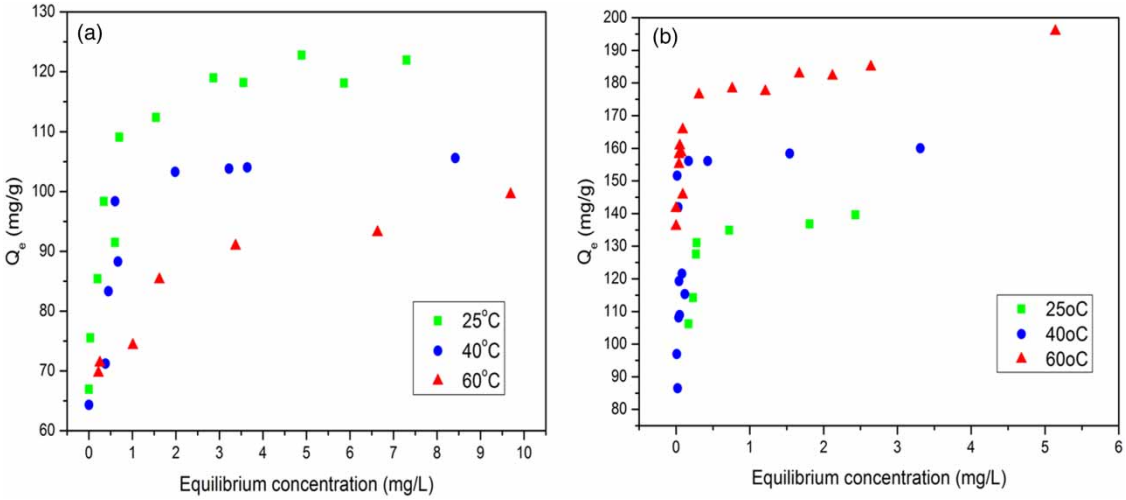

Figure 2 | Liquid phase adsorption isotherms of MB on (a) TiNT and (b) TiNP.

Table 2 | Adsorption isotherm data for MB on TiNT and TiNP

		Langmuir isotherm			BET isotherm		
Morphology	**T (°C)**	K_L	Q_m	r^2	X_m	**A**	r^2
TiNT	25	11.74	122.25	0.999			
	40	9.18	106.84	0.999			
	60	4.16	101.42	0.997			
TiNP	25	37.08	138.69	0.999	12.21	−3297.47	0.997
	40	−185.13	151.98	0.999	13.51	-1.325×10^6	0.998
	60	25.16	193.05	0.998	15.69	−842	0.998

isotherm indicates multilayer adsorption. The TiNP data are a good fit for the BET model, with a calculated monolayer capacity of 15 mg/g, which is in keeping with the theoretically calculated value from the SSA data. The calculated adsorption capacity maximums for the nanotubes using the Langmuir model were 122.65, 106.84 and 101.42 mg/g at 25, 40 and 60 °C, respectively.

The experimental adsorption capacities measured in 100 mL of 10 mg/L MB solution at 25 °C were found to be 120 mg/g for TiNT and 130 mg/g for TiNP samples. This is in good agreement with the Langmuir calculated values for the TiNT sample. The Langmuir model gives lower capacities than observed, however, this model is mostly suitable for monolayer adsorption.

The value of the zeta potential is a measure of the charge on the electric double layer, but can be taken as the surface charge. Therefore, TiNP have a higher –ve surface charge, and attract the positively charged MB ions more strongly. This stronger interaction, along with the flat plate structure compared to the curved tube structure results in the formation of multilayers of MB, and only monolayers in the TiNT adsorption. The lower surface charge may be a result of the scroll structure 'hiding' some of the surface within the tube, where it is balanced by H^+ and Na^+ ions and does not contribute to the surface negativity in the zeta potential measurement. There may also be a contribution from the lowering of strain through layer coupling in the scroll structure. However, this will require further investigation.

As can be seen from Figure 2(a), the adsorbed amount for TiNT decreases with increasing temperature, that is to say, the reaction is an exothermic process. In the case of TiNP, the adsorbed amount increases with increasing temperature, and therefore the adsorption reaction is endothermic in nature. Physical adsorption is generally an exothermic process, however endothermic adsorptions of MB have been reported on activated carbons and clays

(Lin & Teng 2002; Hong *et al.* 2009). Because of this interesting observation, the adsorption was investigated further.

The heats of adsorption, ΔH, were calculated from the van 't Hoff equation (Equation (5)) and are $-39.83\ kJmol^{-1}$ for TiNT and $+25.98\ kJmol^{-1}$ for TiNP. These values indicate a physical adsorption, which is generally of the range $<40\ kJmol^{-1}$ (Lin & Teng 2002). The Gibbs free energy was calculated from Equation (10), and was –ve for both morphologies, indicating a spontaneous reaction in both cases. The values of ΔG at different temperatures are listed in Table 3. The change in entropy for both systems was also calculated as -86 and $130\ JK^{-1}\ mol^{-1}$ for TiNT and TiNP, respectively. The different signs of the entropy for both reactions is interesting. The numerical values are both relatively small, and around the order of values seen for phase changes. Both reactions are spontaneous, as shown by the negative values of the Gibbs energy. A decrease in entropy for an adsorption process would be expected, as is seen for the TiNT, where the negative entropy change is accounted for by the increase in order of the system through adsorption, as the condensed state is more ordered than in bulk solution. The exothermic nature of the adsorption overcomes the increase in order to give a negative value of Gibbs energy, and a spontaneous reaction. The positive value of ΔS for TiNP overcomes the exothermic value of ΔH, resulting in a negative Gibbs energy and a spontaneous reaction. This entropy change reflects the affinity of the plates for the dye and suggests some structural changes in the system. The adsorption of MB will result in a negative change in entropy, however each MB will replace several water molecules, resulting in an overall positive entropy change for the system (Hong *et al.* 2009).

Assuming that MB molecules can occupy the entire surface area, we can calculate the maximum amount of MB adsorbed in a monolayer (Hong *et al.* 2009). Rather than lying flat on the surface, MB has been shown to adsorb onto clay surfaces at a tilted angle (Krishna *et al.* 2004). The dimensions of an MB molecule are given as 1.65 nm by 0.77 nm wide and 0.4 nm thick. Therefore, the area that one molecule of MB takes up on a surface can therefore vary from $1.27\ nm^2$ for flat lying cations to $0.66\ nm^2$ for molecules perpendicular to the surface. These values correspond to a capacity of 102–240 mg/g for TiNT and 16.4–38.6 mg/g for TiNP. From these figures, we can conclude that MB is adsorbed on the nanotube surface in a monolayer at a low tilting angle, whereas the adsorption mode for the nanoplates appears to be multilayer adsorption, with not enough surface layer available to provide the high capacity observed in a monolayer configuration.

The adsorption capacities of the TiNT and TiNP were compared with similar complex nanomaterials in the literature, shown in Table 4. Both materials showed a favourable adsorption capacity.

Table 3 | Thermodynamic parameters for adsorption of MB on TiNT and TiNP

Morphology	$\Delta H\ (kJmol^{-1})$	T (°C)	$\Delta G\ (kJmol^{-1})$	$\Delta S\ (kJmol^{-1})$
TiNT	−39.83	25	−14.04	−86.68
		40	−12.7	−86.68
		60	−10.97	−86.67
TiNP	25.98	25	−12.965	130.7
		40	−15.34	132.0
		60	−17.56	130.75

Kinetics of adsorption

The kinetics of the adsorption process for both morphologies was examined using the linear form of the pseudo-second-order model, shown in Figure 3. The suitability of the model to the data was determined from the correlation coefficients of the linear regression, r^2. In both cases, the coefficients are >0.99, indicating a good fit. The kinetic parameters are listed in Table 5. Figure 4 shows the plots of the adsorption process using the intraparticle diffusion model. For TiNT, the two-phase plot suggests that the adsorption proceeds by external mass transfer or boundary layer diffusion, which is described by the curved section of the plot, and intraparticle or pore diffusion described by the linear section. TiNP exhibits a linear plot, indicating that pore diffusion governs the process. The slope of the linear portion of the plot is defined as the intraparticle diffusion parameter, k_i. The values are

Table 4 | Comparison of adsorption capacities of complex nanomaterials for MB

Adsorbent	Experimental adsorption capacity (mg/g)	Reference
Carbon nanotubes	35.4–64.7	Yao *et al.* (2010)
Magnetite loaded carbon nanotubes	48.06	Ai *et al.* (2011)
Carbon nanotube aerogels	62.5	Tabrizi & Yavari (2015)
Halloysite nanotubes	84.32	Zhao & Liu (2008)
NiO/MCM-41 composite	23.26	Xiao *et al.* (2015)
TiNT and TiNP	120, 130	This study

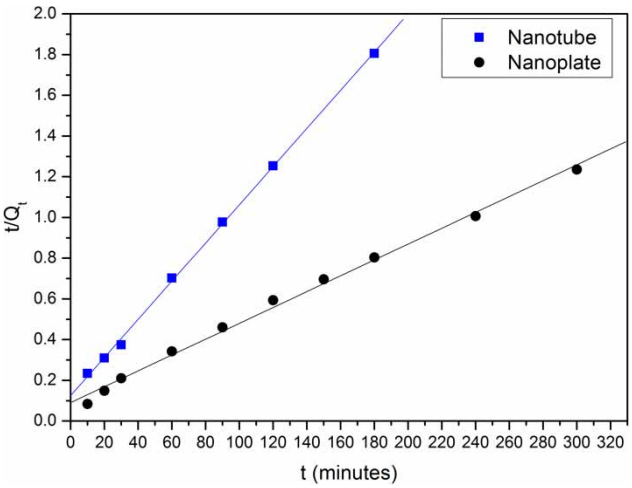

Figure 3 | Pseudo-second-order kinetics of MB onto TiNP and TiNT.

Table 5 | Kinetic data for the adsorption of MB on TiNT and TiNP

	TiNT	TiNP
Pseudo second order		
Q_e, mg/g	106.61	257.07
k_{ps}, g/mg min	7.05×10^{-4}	1.67×10^{-4}
r^2	0.999	0.995
Intraparticle diffusion		
k_i (mg/(gmin$^{0.5}$))	2.54	10.37

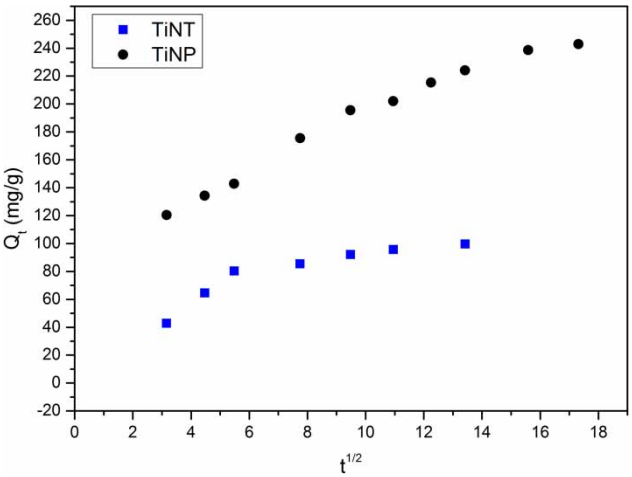

Figure 4 | Diffusion model plots for TiNT and TiNP adsorption of MB. Conditions: 10 mg/L 25 °C.

listed in Table 5. The value for TiNP is higher than for TiNT, indicating the intraparticle diffusion occurs faster for the TiNP sample.

After the capacity of adsorption was reached, the particles aggregated and deposited on the base of the beaker. This is an interesting property for applications of water treatment where separation of the adsorbant is an issue. This occurs because the adsorption is an electrostatic interaction, and repulsion between the particles helps in stabilising the suspension. When the charge is neutralized by MB adsorption, the particles aggregate and deposit on the base of the vessel. The adsorption capacities of macrosized bulk TiO_2 and $H_2Ti_3O_7$ was also measured and found to be negligible. During the measurements of adsorption, the sample was suspended in the MB solution by sonication. After adsorption, the particles aggregated together to form m sized clumps and deposited on the bottom of the vessel. As a comparison, TiNT dispersed in water aggregate and deposit over hours, but TiNT after MB adsorption aggregate and deposit within 5 min.

CONCLUSIONS

Two distinct trititanate nanomorphologies were prepared by the hydrothermal treatment of TiO_2 with strong base. The two morphologies, plates and tubes, had very different structural and adsorption properties. Nanotubes with high surface area and pore volume exhibited exothermic monolayer adsorption of MB. Nanoplates with low surface area and pore volume nanoplates yielded a higher adsorption capacity through endothermic multilayer adsorption governed by pore diffusion. The stronger electrostatic interaction between the TiNP surface and the MB molecules results in multilayer adsorption, and the different modes of adsorption of the two morphologies result in the exothermic and endothermic character for TiNT and TiNP, respectively.

The morphology dependent adsorption characteristics of two materials prepared by a facile and low cost production method have interesting potential applications in wastewater treatment. It is also interesting and informative to observe such different adsorption properties within the same material phase of different nanomorphologies.

ACKNOWLEDGEMENTS

We would like to thank the Fellowship for Young International Scientists from Chinese Academy of Sciences, National Science Foundation of China (50950110349 and 10704051), and Xi'an Jiaotong Liverpool University Research Development fund.

REFERENCES

Ai, L., Zhang, C., Liao, F., Wang, Y., Li, M., Meng, L. & Jiang, J. 2011 Removal of methylene blue from aqueous solution with magnetite loaded multi-wall carbon nanotube: kinetic, isotherm and mechanism analysis. *J. Hazard. Mater.* **198**, 282–290.

Chen, Q., Zhou, W., Du, G. & Peng, L. M. 2002 Trititanate nanotubes made by a single alkali treatment. *Adv. Mater.* **14**, 1208–1211.

Crini, G. 2006 Non-conventional low-cost adsorbents for dye removal: a review. *Bioresour. Technol.* **97**, 1061–1085.

Dawson, G., Chen, W., Zhang, T., Chen, Z. & Cheng, X. 2010 A study on the effect of starting material phase on the production of trititanate nanotubes. *Solid State Sci.* **12**, 2170–2176.

Dawson, G., Liu, J., Lu, L. & Chen, W. 2012 Dopamine-modified trititanate nanotubes with UV- and visible-light photocatalytic activity: coordinative self-assembly into a recyclable absorber. *Chem. Chat. Chem.* **4**, 1133–1138.

El-Halwany, M. M. 2010 Study of adsorption isotherms and kinetic models for methylene blue adsorption on activated carbon developed from Egyptian rice hull. *Desalination* **250**, 208–213.

Feldman, Y., Wasserman, E., Srolovitz, D. J. & Tenne, R. 1995 High-rate, gas-phase growth of MoS_2 nested inorganic fullerenes and nanotubes. *Science* **267**, 222–225.

Goldberger, J., He, R., Zhang, Y., Lee, S., Yan, H., Choi, H. J. & Yang, P. 2003 Single crystal gallium nitride nanotubes. *Nature* **422**, 599–602.

Ho, Y. S. & McKay, G. 1999 Pseudo-second-order model for sorption processes. *Process Biochem.* **34**, 451–465.

Hong, S., Wen, C., He, J., Gan, F. & Ho, Y. S. 2009 Adsorption thermodynamics of methylene blue onto bentonite. *J. Hazard. Mater.* **167**, 630–633.

Hoyer, P. 1996 Formation of a titanium dioxide nanotube array. *Langmuir* **12**, 1411–1413.

Hsieh, C. T., Fan, W. S. & Chen, W. Y. 2008 Impact of mesoporous pore distribution on adsorption of methylene blue onto titania nanotubes in aqueous solution. *Microporous Mesoporous Mater.* **116**, 677–683.

Kasuga, T., Hiramatsu, M., Hoson, A., Sekino, T. & Niihara, K. 1998 Formation of titanium oxide nanotube. *Langmuir* **14**, 3160–3163.

Kasuga, T., Hiramatsu, M., Hoson, A., Sekino, T. & Niihara, K. 1999 Titania nanotubes prepared by chemical processing. *Adv. Mater.* **11**, 1307–1311.

Krishna, B. S., Mahadevaiah, N., Murty, D. S. R. & Jia Prakash, B. S. 2004 Surfactant immobilized interlayer species bonded to montmorillonite as recyclable adsorbent for lead ions. *J. Colloid Interface Sci.* **271**, 270–276.

Lee, C. K., Liu, S. S., Juang, L. C., Wang, C. C., Lyu, M. D. & Hung, S. H. 2007 Application of titanate nanotubes for dyes adsorptive removal from aqueous solution. *J. Hazard. Mater.* **148**, 756–760.

Lin, Y. R. & Teng, H. 2002 Mesoporous carbons from waste tire char and their application in wastewater discoloration. *Microporous Mesoporous Mater.* **54**, 167–174.

Liu, R., Fu, X., Wang, C. & Dawson, G. 2016 Dopamine surface modification of trititanate nanotubes: proposed in-situ structure models. *Chem. Eur. J.* **22**, 6071–6074.

Nakamura, H. & Matsui, Y. 1995 Silica gel nanotubes obtained by the sol-gel method. *J. Am. Chem. Soc.* **117**, 2651–2652.

Namane, A., Mekarzia, A., Benrachedi, K., Belhaneche-Bensemra, N. & Hellal, A. 2005 Determination of the adsorption capacity of activated carbon made from coffee grounds by chemical activation with $ZnCl_2$ and H_3PO_4. *J. Hazard. Mater.* **B119**, 189–194.

Parida, S. K., Dash, S., Patel, S. & Mishra, B. M. 2006 Adsorption of organic molecules on silica surface. *Adv. Colloid Interf. Sci.* **121**, 77–110.

Parker, G. R. 1995 Optimum isotherm equation and thermodynamic interpretation for aqueous 1,1,2-trichloroethane adsorption isotherms on three adsorbents. *Adsorption* **1**, 113–132.

Pu, L., Bao, X., Zou, J. & Feng, D. 2001 Individual alumina nanotubes. *Angew. Chem. Int. Ed.* **40**, 1490–1493.

Ramakrishna, K. R. & Viraraghavan, T. 1997 Dye removal using low cost adsorbents. *Water Sci. Technol.* **36**, 189–196.

Tabrizi, N. S. & Yavari, M. 2015 Methylene blue removal by carbon nanotube based aerogels. *Chem. Eng. Res. Des.* **94**, 516–523.

Tenne, R., Margulis, L., Genut, M. & Hodes, G. 1992 Polyhedral and cylindrical structures of tungsten disulphide. *Nature* **360**, 444–446.

Wang, S., Li, H. & Xu, L. 2006 Application of zeolite MCM-22 for basic dye removal from wastewater. *J. Colloid Interface Sci.* **295**, 71–78.

Widjaja, T., Miyata, T., Nakano, Y., Nishijima, W. & Okado, M. 2004 Adsorption capacity of powdered activated carbon for 3,5-dichlorophenol in activated sludge. *Chemosphere* **57**, 1219–1224.

Xiao, X., Zhang, F., Feng, Z., Deng, S. & Wang, Y. 2015 Adsorptive removal and kinetics of methylene blue from aqueous solution using NiO/MCM-41 composite. *Physica E* **64**, 4–12.

Yao, Y., Xu, F., Chen, M., Xu, Z. & Zhu, Z. 2010 Adsorption behavior of methylene blue on carbon nanotubes. *Bioresour. Technol.* **101**, 3040–3046.

Zhao, M. & Liu, P. 2008 Adsorption behavior of methylene blue on halloysite nanotubes. *Microporous Mesoporous Mater.* **112**, 419–424.

First received 8 June 2016; accepted in revised form 27 October 2016. Available online 14 November 2016